Journal of Sound and Vibration 329 (2010) 2158–2176

Contents lists available at ScienceDirect

Journal of Sound and Vibration

journal homepage: www.elsevier.com/locate/jsvi

The use of a hybrid model to compute the nonlinear acoustic performance of silencers for the finite amplitude acoustic wave

Daehwan Kim, Cheolung Cheong *, Weui Bong Jeong

School of Mechanical Engineering, Pusan National University, 30 Jangjeon-dong, Guemjeong-gu, Pusan 609-735, Republic of Korea

ARTICLE INFO

Article history:
Received 6 December 2008
Received in revised form
13 November 2009
Accepted 6 December 2009
Handling Editor: L.G. Tham
Available online 6 January 2010

ABSTRACT

In the present study, a hybrid method is proposed for predicting the acoustic performance of a silencer for a nonlinear wave. This method is developed by combining two models: (i) a frequency-domain model for the computation of sound attenuation due to a silencer in a linear regime and (ii) a wavenumber space model for the prediction of the nonlinear time-evolution of finite amplitudes of the acoustic wave in a uniform duct of the same length as the silencer. The present method is proposed under the observation that the physical process of the nonlinear sound attenuation phenomenon of a silencer may be decoupled into two distinct mechanisms: (a) a linear acoustic energy loss that owes to the mismatch in the acoustic impedance between reactive elements and/or the sound absorption of acoustic liners in a silencer; (b) a nonlinear acoustic energy loss that is due to the energy-cascade phenomenon that arises from the nonlinear interaction between components of different frequencies. To establish the validity of the present model for predicting the acoustic performance of silencers, two model problems are considered. First, the performance of simple expansion mufflers with nonlinear incident waves has been predicted. Second, proposed method is applied for computing nonlinear acoustic wave propagation in the NASA Langley impedance duct configuration with ceramic tubular liner (CT57). Both results obtained from the hybrid models are compared with those from computational aero-acoustic techniques in a time–space domain that utilize a high-order finite-difference method. Through these comparisons, it is shown that there are good agreements between the two predictions. The main advantage of the present method is that it can effectively compute the nonlinear acoustic performance of silencers in nonlinear regimes without time–space domain calculations that generally entail a greater computational burden.

1. Introduction

Silencers are noise control devices that are most frequently used to attenuate the propagation of sound energy in a duct from certain sources and to finally control the radiated noise. The prediction of the performance of a silencer, which is generally described in terms of the transmission loss (TL) and the insertion loss (IL), is essential at the design stage.

The methods that are used for predicting the acoustic performance of a silencer may be divided into two categories: semi-analytic methods and purely numerical methods. Among semi-analytic methods, the transfer matrix method (TMM) that is based on plane wave theory has been widely used to compute the performance of a silencer. The TMM can be used to predict the TL of a silencer that has many reactive elements, such as extended inlets/outlets and perforated walls. Each

* Corresponding author. Tel.: +82 51 510 3205.
E-mail address: ccheong@pusan.ac.kr (C. Cheong).

0022-460X/$ - see front matter © 2009 Elsevier Ltd. All rights reserved.
doi:10.1016/j.jsv.2009.12.010

transfer matrix of reactive elements is well-described in Munjal's work [1]. To further consider higher-order acoustic modes, improved semi-analytic solutions have been developed [2–4]. As purely numerical methods, the boundary element method (BEM) and finite element method (FEM) have been used to estimate the acoustic performance of silencers in the frequency domain [5]. Actually, most studies for predicting the acoustic performance of silencers in related industries are nowadays conducted by using commercial programs that employ BEM and FEM modules. However, all these methods are based on acoustically linear approximations, as a result of which the methods are limited to the prediction of the linear acoustical behaviors of silencers.

As the speed of flow increases due to the demand for greater efficiency, the operating range of silencers more frequently involves nonlinear regimes where the magnitude of incident disturbance is so large that a linear approximation may not be valid any more. For example, the sound pressure level (SPL) of inlet fan noise generated from aero-engines can go beyond 160 dB near the fan face so that the nonlinear behavior of finite amplitude acoustic waves is important consideration. In this circumstance, the acoustic performance of a silencer used to attenuate inlet fan noise may not be properly predicted through the traditional linear approaches.

For the prediction of the performance of a silencer in a nonlinear regime, the nonlinear gas dynamic models have been utilized to characterize the behavior of high sound level in time–space domain [6–10]. The time–space domain method is more useful for understanding the nonlinear acoustic field and its physics, since this method is similar to actual experiments [11]. In the previous studies, the sound attenuation phenomena due to resistive and reactive parts in a silencer are computed by utilizing this advantage of time–space domain methods. Tam et al. [12] computed the reflection of the silt resonator by using a high-order finite-difference-method (FDM) in the time–space domain; his findings agreed well with experimental results. Using similar methods, the absorption of sound by an in-duct orifice was investigated, where the strength of vortex shedding on both sides of the orifice is shown to determine the levels of absorption [13]. Dickey et al. [14] investigated the acoustic behavior of a perforated tube silencer at a high level of sound. Hwang et al. [11] calculated the IL of an exponential pipe silencer for an *N*-wave of a single frequency. Cho and Lee [15] predicted nonlinear acoustic propagation in a lined duct for single frequency sinusoidal and saw-tooth waves. These works demonstrate that time–space domain methods are more attractive than traditional frequency-domain approaches for analyzing nonlinear acoustic performance and understanding the related physics.

However, due to physical and numerical issues [16,17], it is challenging for engineers who work in related industrial fields to apply the time–space domain computational aero-acoustic techniques for the assessment of the acoustic performance of silencers. Acoustic waves are intrinsically unsteady, their amplitudes are several orders smaller than the mean flow and their frequencies are generally very high. Thus, to ensure that the computed solution is uniformly accurate over the entire computational domain, the numerical scheme must be free of numerical dispersion, dissipation and anisotropy. Simultaneously, the important, nonreflecting boundary condition is addressed for its application in duct acoustics, e.g., silencers, since the solution in the physical domain is more susceptible to the contamination of the reflected waves from the boundary of the computational domain. This is due to the intrinsic characteristics of the internal flows: the distance between the sources of sound and the boundary is generally short and no asymptotic solutions are allowed.

In present study, for circumventing such difficulties in the use of numerical methods in the time–space domain, a hybrid method is proposed for computing the acoustic performance of silencers for nonlinear incident waves. To develop the hybrid model, two kinds of model problems are considered: TL of a simple expansion muffler subject to high amplitude of incident broadband sound and acoustic wave propagation in a lined duct for the incident sinusoidal waves with finite amplitudes. We first use time-accurate computational aero-acoustic techniques to calculate the TL of simple expansion mufflers that are subjected to incident sound waves with high amplitudes. The result indicates that the physical process involved in the nonlinear TL may be decoupled into two distinct mechanisms: (a) a linear TL that owes to the mismatch in the impedance of connected ducts in the muffler due to the differing cross-sectional areas and (b) a nonlinear TL that is due to the phenomenon of the cascade of energy from lower-frequency components to higher ones. Further application of time–space method for predicting nonlinear acoustic propagation in the lined duct also shows that the SPL variation along the duct is also due to two distinct mechanisms: (a) sound absorption by the acoustic liners and (b) generation of harmonics of initial sinusoidal wave by the nonlinear energy cascade between the harmonic waves. Based on these observations, the hybrid method is proposed, which consists of two steps for predicting the nonlinear acoustic attenuation in silencers. First, the linear sound absorption of the silencer is predicted by using a traditional linear-approximation method in the frequency-domain. Second, this linear performance of silencer is corrected with nonlinear acoustic wave propagation in a uniform duct that is of the same length as the silencer; this nonlinear solution of the uniform duct is computed in the wavenumber space through the time-evolution integration of the initial wave. To validate the present approach, the predictions of the nonlinear TL of mufflers and sound pressure level (SPL) along the wall of the lined duct from the hybrid method are compared with those from time–space domain methods. The main advantage of the present approach is that it can effectively compute the nonlinear attenuation of acoustic waves through silencers without time–space domain analysis entailing a greater computation burden.

In the following section, the computational aero-acoustic techniques in time–space domain are applied for understanding the mechanism of nonlinear wave attenuation by the reactive and resistive parts of silencers. In Section 3, the hybrid method is described with the detailed computational procedures for predicting the acoustic performance of silencers for the incident nonlinear waves. The predicted results from the hybrid and time–space domain methods are compared and the related issues are discussed in Section 4, followed by the concluding remark.

2. Time–space domain analysis

In this section, the nonlinear performance of silencers subject to finite amplitude of incident acoustic waves is computed by using computational aero-acoustic techniques in the time–space domain. The purpose of the time–space domain analysis is to understand the physical phenomena in the nonlinear sound attenuation. This analysis helps to provide basic principle for the development of the hybrid method in the following section. Two model problems are utilized to assess the nonlinear performances of reactive and resistive parts in silencers: (Problem 1) nonlinear TLs of simple expansion mufflers for the incident nonlinear acoustic wave; (Problem 2) nonlinear acoustic wave propagation in a lined duct for high amplitude of incoming sinusoidal wave.

2.1. Governing equations and model problems

In this paper, density (ρ), velocity (u, v) and pressure (p) are non-dimensionalized by ρ_∞, c_∞ and $\rho_\infty c_\infty^2$, respectively. Here, ρ_∞(=1.225 kg/m^3) and c_∞(=340 m/s) denote the ambient density and speed of sound, respectively. The space coordinates and time (t) are normalized by characterized length scales, Δx(=Δy) and $\Delta x/c_\infty$, respectively.

Problem 1. Nonlinear TLs of simple expansion mufflers for the incident nonlinear acoustic pulse.

The nonlinear acoustic performance of simple expansion mufflers is first predicted in terms of the TL. We consider two simple expansion mufflers that are axi-symmetrically cylindrical. Fig. 1 shows a cross-section of these two models. As governing equations, the unsteady axisymmetric compressible Euler equations are employed in the following form:

$$\frac{\partial \rho}{\partial t}+\rho\frac{\partial u}{\partial x}+\rho\frac{\partial v}{\partial r}+u\frac{\partial \rho}{\partial x}+v\frac{\partial \rho}{\partial r}+\frac{1}{r}\rho v=0, \tag{1}$$

$$\frac{\partial u}{\partial t}+u\frac{\partial u}{\partial x}+v\frac{\partial u}{\partial r}+\frac{1}{\rho}\frac{\partial p}{\partial x}=0, \tag{2}$$

$$\frac{\partial v}{\partial t}+u\frac{\partial v}{\partial x}+v\frac{\partial v}{\partial r}+\frac{1}{\rho}\frac{\partial p}{\partial r}=0, \tag{3}$$

$$\frac{\partial p}{\partial t}+u\frac{\partial p}{\partial x}+v\frac{\partial p}{\partial r}+\gamma p\frac{\partial u}{\partial x}+\gamma p\frac{\partial v}{\partial r}+\frac{1}{r}\gamma p v=0, \tag{4}$$

where γ is specific heat ratio. Coordinates (x, r) are nondimensionlized by length scale, Δx=Δr=2.5 mm.

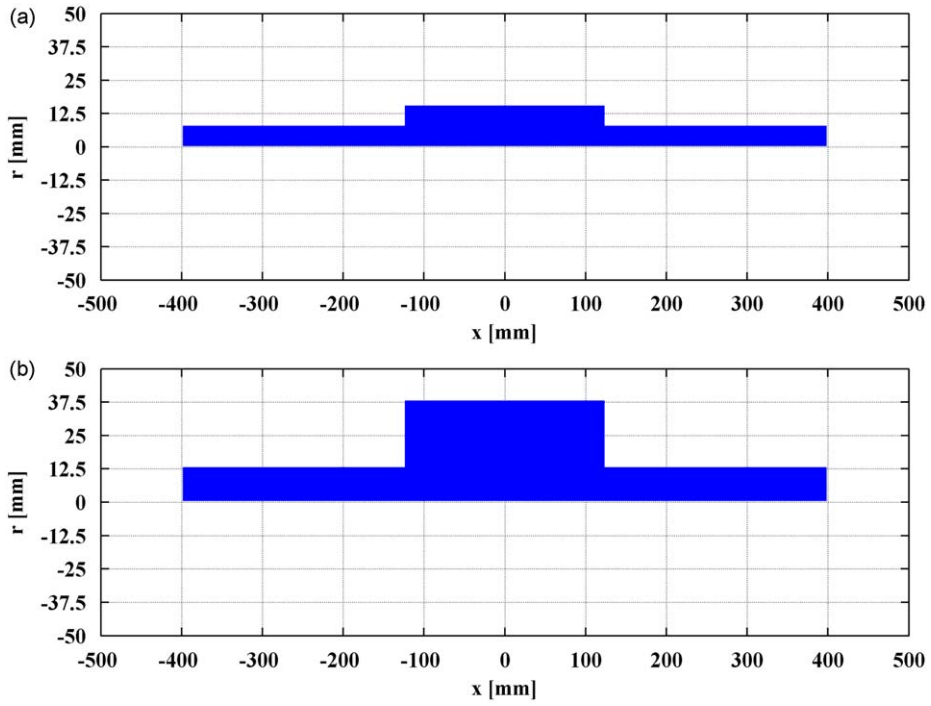

Fig. 1. Cross-section of the two simple expansion mufflers under study and their dimensions: (a) Muffler #1 (diameter=30.75 mm and area ratio=3.8) and (b) Muffler #2 (diameter=76.25 mm and area ratio=8.4).

The first muffler has a chamber of diameter, 30.75 mm, and its area ratio is 3.8. For the second muffler, the chamber diameter and the area ratio are set to 76.25 mm and 8.4, respectively. The cut-off frequency of the first radial mode in the first muffler is 6476 Hz, while that of the second muffler is 2612 Hz. This means that the former muffler allows acoustic waves to maintain plane waves in its chamber in the frequency range until 6476 Hz, while the latter muffler does not do so. The reason for this choice will be described in Section 4. The lengths of the whole ducts and the chamber are 800 and 250 mm, respectively, which are the same in both mufflers. For convenience, the mufflers are respectively numbered 1 and 2 in the subsequent sections.

Problem 2. Nonlinear acoustic wave propagation in a lined duct for high amplitude of sinusoidal wave.

The nonlinear acoustic performance of a lined duct is also analyzed. The NASA Langley impedance duct with a CT57 liner is used for the second simulation. The configuration of impedance duct is shown in Fig. 2. The acoustic performance of a lined duct is predicted in two-dimensional computation. The unsteady compressible Euler equations are utilized in Cartesian coordinates

$$\frac{\partial \rho}{\partial t}+\rho\frac{\partial u}{\partial x}+\rho\frac{\partial v}{\partial y}+u\frac{\partial \rho}{\partial x}+v\frac{\partial \rho}{\partial y}=0, \tag{5}$$

$$\frac{\partial u}{\partial t}+u\frac{\partial u}{\partial x}+v\frac{\partial u}{\partial y}+\frac{1}{\rho}\frac{\partial p}{\partial x}=0, \tag{6}$$

$$\frac{\partial v}{\partial t}+u\frac{\partial v}{\partial x}+v\frac{\partial v}{\partial y}+\frac{1}{\rho}\frac{\partial p}{\partial y}=0, \tag{7}$$

$$\frac{\partial p}{\partial t}+u\frac{\partial p}{\partial x}+v\frac{\partial p}{\partial y}+\gamma p\frac{\partial u}{\partial x}+\gamma p\frac{\partial v}{\partial y}=0, \tag{8}$$

The height of duct (H) is 50.8 mm and the length of duct equals $16\times H$. The Cartesian coordinates (x, y) are scaled by length scale, $\Delta x=\Delta y=1.016$ mm. Δx and Δy are grid spacing in x- and y-direction. This spacing equals $1/50\times H$.

2.2. Numerical algorithms

To compute nonlinear acoustic fields for the model problems in time-domain, Euler equations are solved by using a time-accurate high-order FDM where a seven-point DRP scheme [18] is applied for spatial discretization and the optimized Adams–Bashford method is used for the time-marching. The slip condition is applied to all of the expansion muffler walls with the ghost points of Tam and Dong [19]. Numerical spurious short waves are known to be generated in discontinuous boundaries [20], such as the corners of suddenly enlarged, contracted chambers and different boundary condition, in the computational domain. Therefore, the artificial selective damping terms [18] are applied to the discretized equations so that the spurious waves are effectively removed. The current numerical schemes have been applied and validated for various applications [20–24].

Predicting internal acoustic field in silencers, nonreflecting boundary condition is essential to prevent its numerical solution from the contamination of unphysical wave reflected from the boundary in computational domain. In the present study, the perfectly matched layer (PML) method is implemented as a nonreflecting boundary condition. The PML with the damping function described in [25,26] is applied to the inlet and outlet buffer regions whose widths equal $200\times\Delta x$. In inlet buffer region, acoustic wave is generated and reflected wave is also absorbed at the same time. Therefore, the inflow and PML boundary condition are applied on the inlet region.

For the simulation of wave propagation in the lined duct, the acoustic performance of the liner is modeled by time-domain broadband impedance boundary condition. The impedance boundary condition is usually modeled in frequency domain, which cannot be directly utilized in time–space domain simulation. Many investigations have been carried out to develop time-domain impedance boundary conditions [27–30]. In this paper, we generally followed the procedure of Özyörük et al. [29]. Detailed implementation procedure and properties of CT57 liner are included in Appendix A.

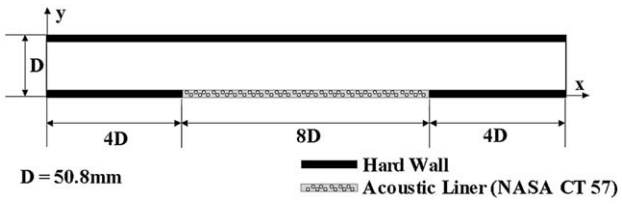

Fig. 2. Two-dimensional schematics of NASA Langley impedance duct with a CT57 liner.

2.3. Effects of the amplitude of incident wave

Considering acoustic waves propagating in a duct, nonlinear phenomenon such as the wave steepening becomes important for the incident wave of amplitude higher than certain critical value. Therefore, preliminary studies are carried out to investigate the effects of the amplitude of incident waves on sound propagation characteristics in a uniform duct.

Problem 1. Nonlinear TLs of simple expansion mufflers for the incident nonlinear acoustic pulse.

The diameter and length of the duct are set to 15.75 and 800 mm, respectively. The acoustic pulse is generated at the inlet boundary according to a Gaussian distribution of the form

$$p = p_\infty + h\exp[-\ln 2(x/b)^2], \tag{9}$$

where h is the amplitude of the Gaussian distribution and b determines the width of the distribution. Here, p and p_∞ (=101,325 Pa) represent total pressure and ambient pressure, respectively. Fig. 3 represents the results of acoustic initial pulse propagation of fluctuation value for the initial pulse that is defined in Eq. (9), where $h/\rho_\infty c_\infty^2$ is set to 0.0005 and 0.05, respectively, for the linear and nonlinear incident waves, while the value of $b/\Delta x$ is fixed at 10. The SPL of the linear and nonlinear incident waves correspond to 130 and 170 dB, respectively.

It can be seen that wave retains its initial shape for $h/\rho_\infty c_\infty^2$=0.0005, as shown in Fig. 3a, while the nonlinear wave propagation characteristics occur for the incident wave of $h/\rho_\infty c_\infty^2$=0.05 in Fig. 3b. These values of the amplitudes of the incident wave are utilized in the subsequent simulation for the prediction of the TLs of the two mufflers. The former value ($h/\rho_\infty c_\infty^2$=0.0005) is for linear TL and the latter ($h/\rho_\infty c_\infty^2$=0.0005) is for nonlinear TL. In addition, no reflective waves from the boundary are observable, which ensures the effectiveness of the nonreflective boundary condition that is applied.

Problem 2. Nonlinear acoustic wave propagation in a lined duct for high amplitude of sinusoidal wave.

The uniform duct without a liner has the same dimension as that of the impedance duct shown in Fig. 2. The inflow and PML boundary conditions are applied at inlet buffer region ($-200\Delta x \le x \le 0$) with the form of sinusoidal wave, Amp $\times \sin(kx-\omega t)$. Here, Amp, ω and k denote the amplitude, angular frequency and wavenumber of the incoming wave, respectively. The sinusoidal wave is generated at the frequency 250 Hz with finite amplitude, Amp=$2^{1/2}\, p_{\mathrm{ref}} 10^{\mathrm{SPL}/20}/\rho_\infty c_\infty^2$ where p_{ref}=20 μPa.

As shown in Fig. 4a, the acoustic wave of 130 dB (Amp ≈ 0.00063) travels in the duct without its higher harmonic components in the interesting range of SPL. When the SPL of acoustic wave is set to be 160 dB (Amp ≈ 0.02), however, amplitudes of its harmonic components appear and increase as the wave travels as shown in Fig. 4b. We set the SPL of incident wave to be 130 dB for the linear computation and 160 dB for the nonlinear case.

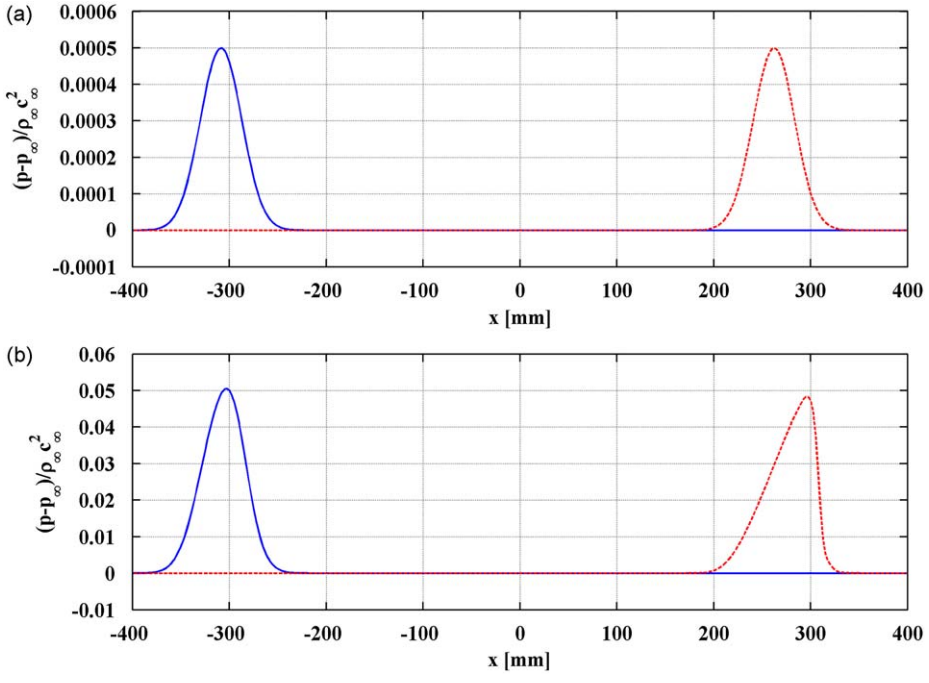

Fig. 3. Linear and nonlinear wave propagation in a uniform duct: (a) linear incident wave ($h/\rho_\infty c_\infty^2$=0.0005) and (b) nonlinear incident wave ($h/\rho_\infty c_\infty^2$=0.05). (——— waveform in the inlet, — — — waveform in the outlet.)

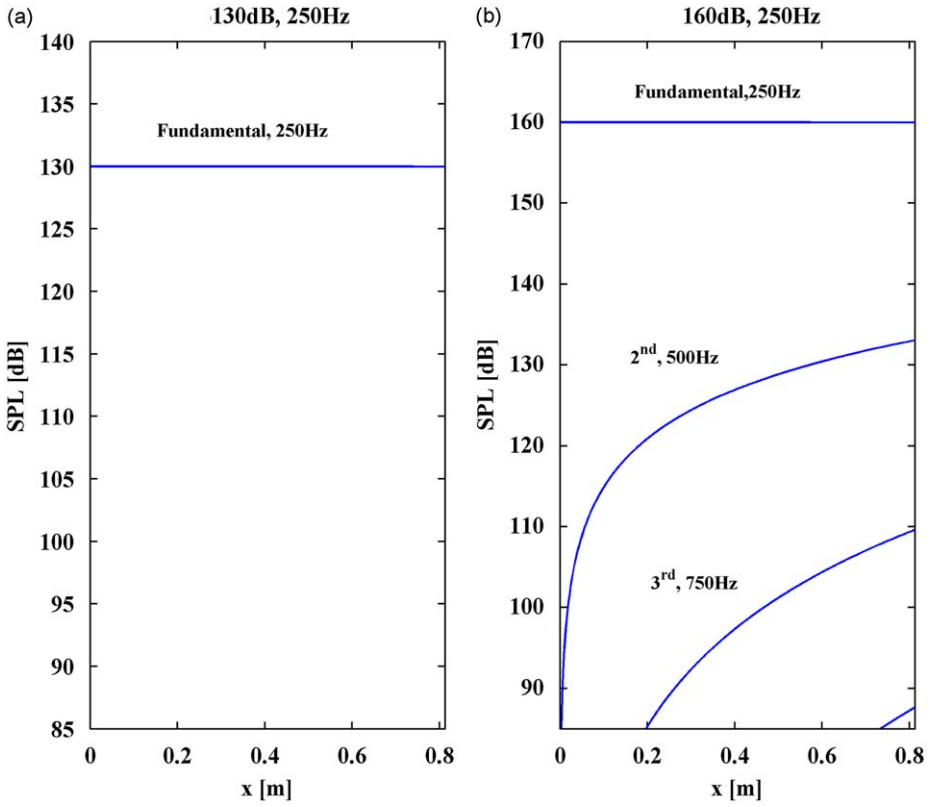

Fig. 4. Variation of SPL for the harmonics of the fundamental frequency at 250 Hz: (a) for 130 dB and (b) for 160 dB.

2.4. Prediction of nonlinear acoustic performance of silencers

Problem 1. Nonlinear TLs of simple expansion mufflers for the incident nonlinear acoustic pulse.

The time–space domain numerical methods, described and applied in the previous section, are utilized to predict the TL of the mufflers shown in Fig. 1. However, the geometry of the mufflers is different from the earlier, uniform duct: there are discontinuous boundaries at the corner of the chambers. It is well-known that spurious numerical waves are generated at discontinuous boundaries [20]. Therefore, artificial selective damping terms [18] are applied to the discretized equations so that the spurious waves are effectively removed. The values of R, mesh Reynolds number in ref. [18], are set lower for grid-points in the discontinuous regions than for those in other regions because the spurious waves are predominantly generated in discontinuous areas. However, extensive numerical testing reveals that the artificial selective damping needs to be cautiously employed in the wall region to avoid non-physical phenomena. This is described in detail in Appendix B.

Generally, TL is defined as below

$$\mathrm{TL} = 10\log_{10}(|I|/|T|)^2. \tag{10}$$

In Eq. (10), I and T, are the peak amplitudes of the incident and transmitted waves at the corresponding frequency. I is the known value and T is unknown and calculated by using the discrete Fourier transform (DFT) of the recorded time history at the outlet point of the muffler, which is set to x=400 mm, as shown in Fig. 1. The predicted TLs of muffler #1 for the incident linear and nonlinear waves are shown in Fig. 5a. It can be seen in Fig. 5a that the linear TL spectrum that is predicted by the use of the time–space domain method shows excellent agreement with that which is predicted by the frequency-domain BEM in the commercial software, SYSNOISE^{TM}. Note that these two predictions show subtle discrepancy which becomes slightly larger as the frequency increases. The similar results were reported in the work of Hwang et al. [11], which explains that the reason for this is due to the time–domain numerical wall boundary condition on the sharp corners of the chamber. This boundary condition makes the sharp corners behave as a little rounded one, which more resembles the real corners, while the prediction in the frequency-domain BEM is executed with the ideal sharp corners. As expected, however, Fig. 5a shows that the overall shape of the predicted TL spectrum for the nonlinear incident wave is different from that under the frequency-domain method. More detailed inspection into the difference reveals that the oscillating TL in the higher-frequency pattern is similar in both results and that the main reason for the difference can be attributed to the lower-frequency oscillation in the time–space domain result. The characteristic of this oscillation is that

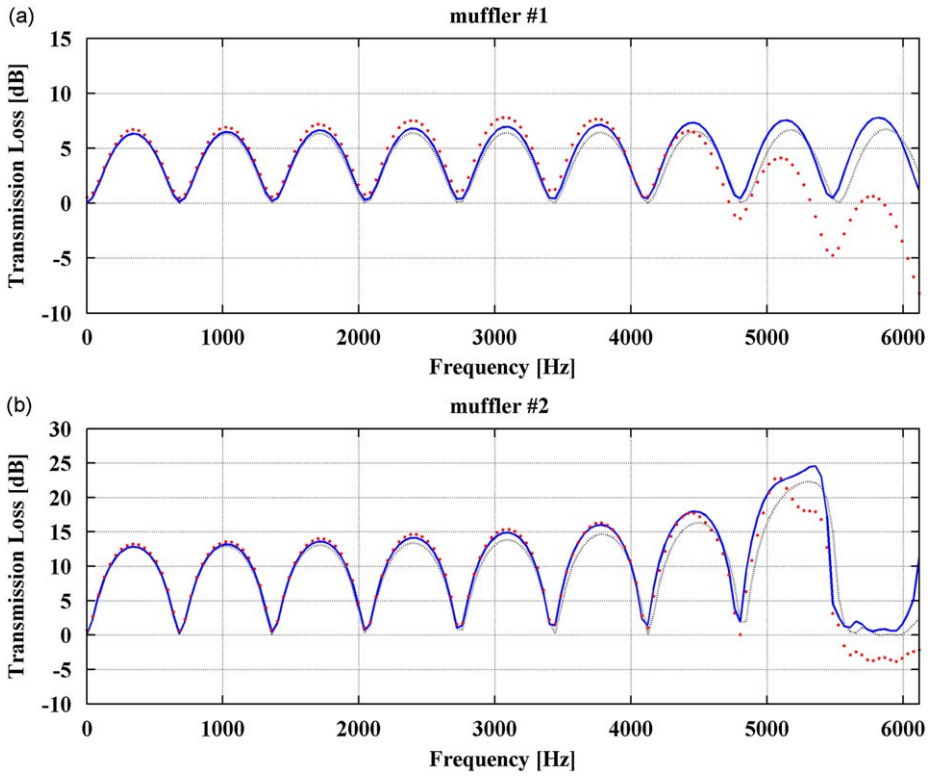

Fig. 5. Comparison of the TLs of muffler #1, for the incident linear and nonlinear waves, which are predicted by the time-space domain and frequency-domain methods: (a) linear TL and (b) nonlinear TL (…… linear TL from the frequency-domain; ——— linear TL from time-space domain; ■ nonlinear TL from time-space domain).

the gain of TL in the lower-frequency range is converted into a loss of TL in the higher-frequency range. The same comparisons are carried out for muffler #2 in Fig. 5b, which shows there is good agreement between the linear TL spectrums that are predicted by the time–space domain and frequency-domain methods. As shown in Fig. 5b, a discrepancy can be observed between the two results for the nonlinear incident wave. However, the reason for the difference is similar to that in Fig. 5a. This similarity strongly suggests that the nonlinear TL may be independent of the detailed geometries of mufflers. As shown in Fig. 3b, a nonlinear incident waveform cannot maintain its initial shape because of the cascade of energy from lower-frequency components to higher ones. It can be expected that this characteristic of nonlinear wave propagation may be involved in the process of wave transmission in the mufflers, which seems to be why the TL spectrums for the nonlinear incident wave have negative TL levels at relatively higher frequencies. To confirm this inference, in Fig. 6, the nonlinear TLs are compared with the values that are obtained by adding the linear TL that is ascertained from FDM to the TL in the uniform duct for the nonlinear incident wave. The respective sets of results for both mufflers are in good agreement.

Problem 2. Nonlinear acoustic wave propagation in a lined duct for high amplitude of sinusoidal wave.

Before computing nonlinear acoustic wave propagation in a lined duct, we tried to validate the present numerical method by the comparison of the predicted SPLs with the experimental data. The computations in the time domain and the NASA experiments were conducted at 6 different frequencies from 0.5 to 3 kHz by 0.5 kHz increments. For the linear case with the incident wave of amplitude 130 dB, the computation results are shown in Fig. 7. It can be seen that there are good agreements between the time–space domain analysis and experimental data.

Subsequently, linear and nonlinear simulations are performed for the incident wave of 250 Hz. Their results are shown in Fig. 8. As already shown in Fig. 4, it is revealed that the harmonics are gradually generated during the propagation of the incident wave of the amplitude of 160dB. In a similar manner, when the liner is present, the 2nd harmonic with 500 Hz is gradually generated and, at the same time, propagates on the liner. This 2nd harmonic, therefore, loses its acoustic energy by the interaction with the liner. Accordingly, the overall shape of SPL variation of the 2nd harmonic along a lined duct grossly follows that (dashed line) of the 2nd harmonic in the case without liner but with slightly decreased amplitudes, as shown in Fig. 8b. This result implies that the characteristic of nonlinear wave propagation may be involved in the process of wave attenuation due to the acoustic liner. The SPLs of the fundamental wave for both cases involving the linear

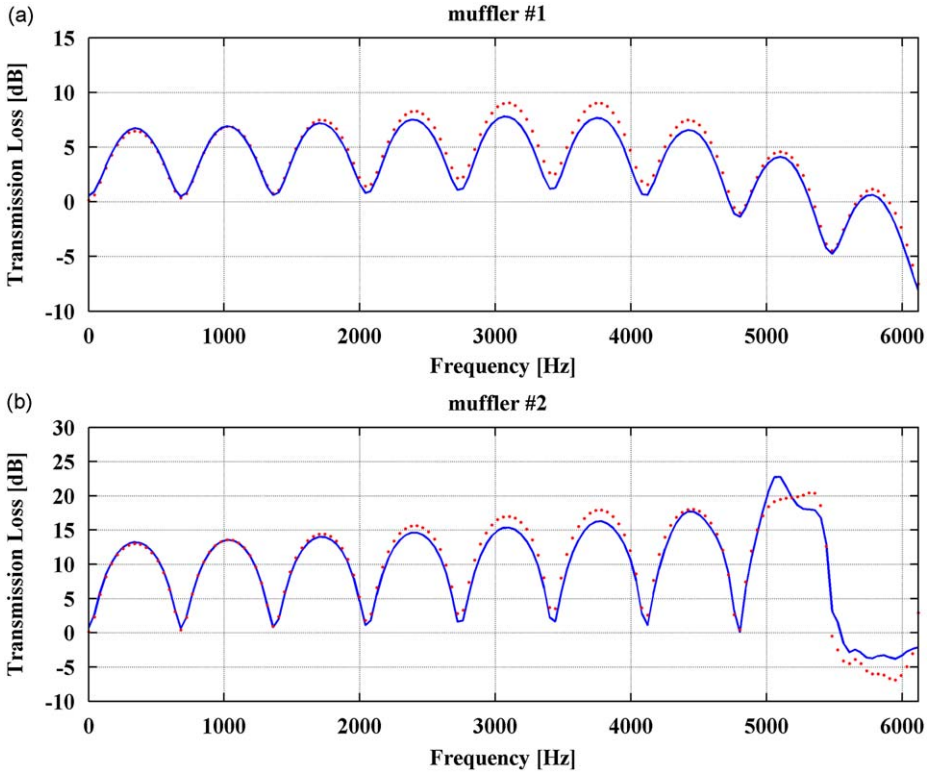

Fig. 6. Comparison of the predicted nonlinear TL in time-domain with that obtained by adding the linear TL using FDM to the TL in the uniform duct for the nonlinear incident wave for: (a) muffler #1 and (b) muffler #2. (——— nonlinear TL_{muffler} from time-space domain; ■ linear TL_{muffler} from time-space domain + nonlinear TL_{duct} from time-space domain).

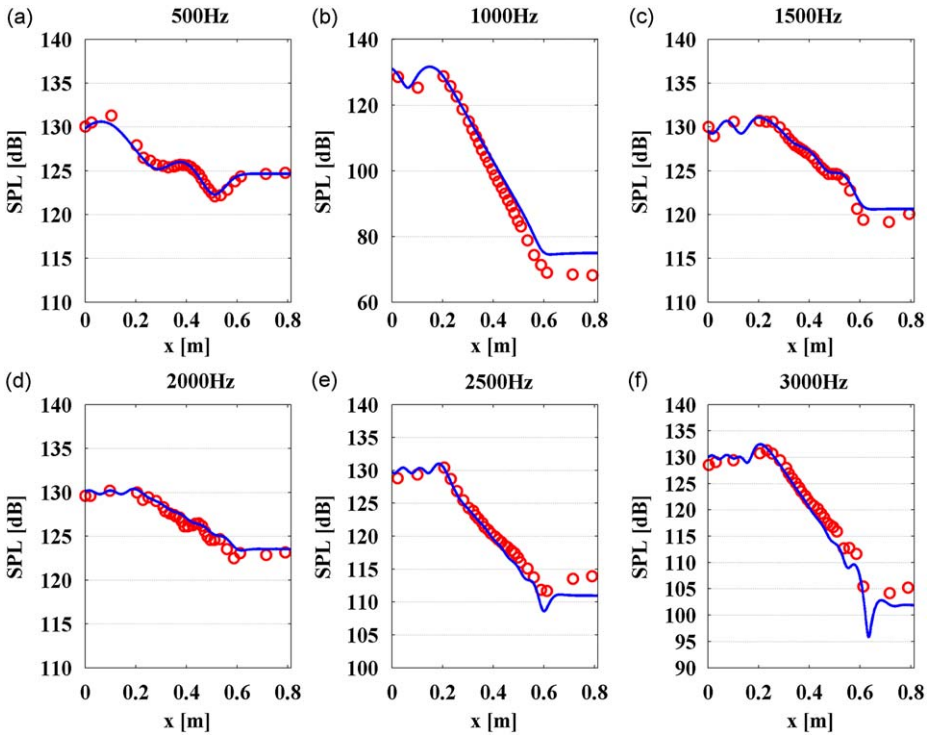

Fig. 7. Comparison of the linear wave propagation results from time-domain analysis with NASA experimental results. (— time-domain analysis for the linear incoming wave; ○ NASA experiment).

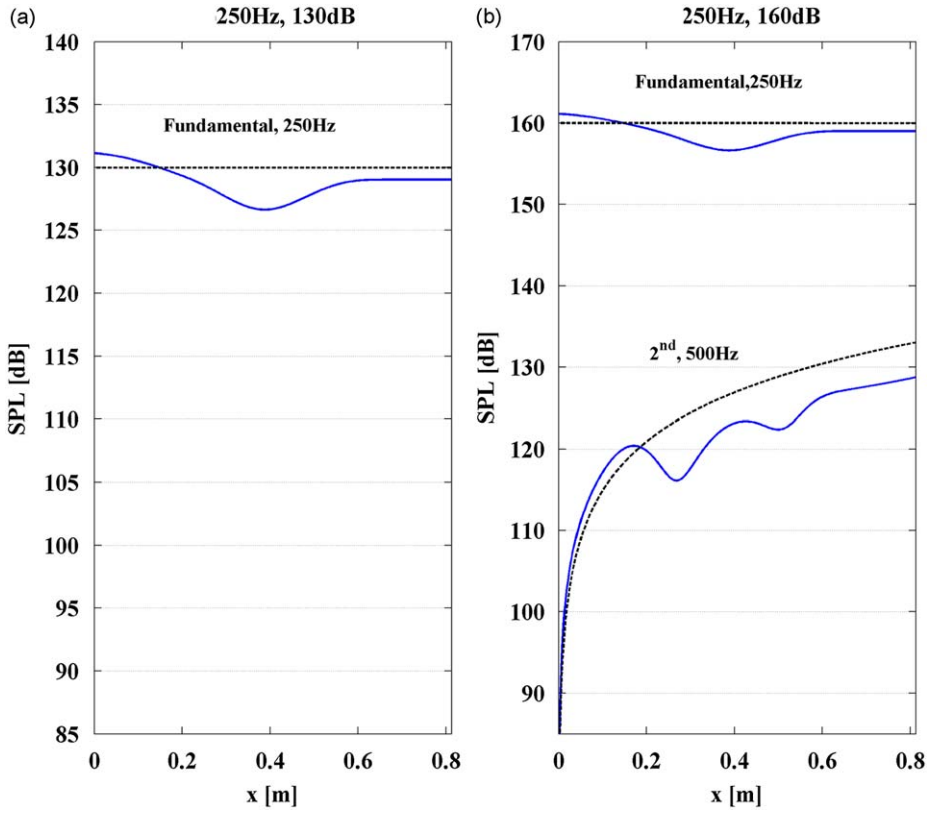

Fig. 8. Predicted wave propagation from time-space domain computation for the linear/nonlinear incoming sinusoidal acoustic wave at 250 Hz: (a) for 130 dB and (b) for 160 dB. (——— with liner, – – – without liner).

and nonlinear incident waves have almost the same patterns. This implies that the attenuation due to the liner is linear and that there is no noticeable loss of acoustic energy of the fundamental wave due to energy cascade from fundamental frequency to its harmonics as shown in Fig. 4. The linear attenuation by the liner is from the numerical boundary condition that employs the same impedance for different sound levels. It can be, however, stated that if the attenuation slope of the experimental data is the same, the impedance is the same. It is interesting to note that the liners' nonlinearity may be neglected for some specific cases [31].

3. Calculation of the nonlinear acoustic performances by using a hybrid model

In Section 2, we computed the nonlinear performance of silencers by using time–space domain methods by which it is shown that the physical process that is involved in the nonlinear sound attenuation phenomenon due to the silencers may be decoupled into two distinct mechanisms: linear attenuation process and nonlinear wave propagation. Based on this observation, a hybrid model is proposed for the effective computation of the nonlinear acoustic performance of silencers. The hybrid model consists of two models: a frequency-domain model for the computation of the linear acoustic performance of silencers in the linear regime and a wavenumber space model for the prediction of the nonlinear time-evolution of finite amplitudes of the acoustic source in a uniform duct of the same length as the silencers. Therefore, the hybrid model is constructed by combining these two models. However, as described in the introduction, various methods such as TMM, BEM and FEM, are available for computing the linear performance of silencers. Therefore, in this section, we focus on the computation of the nonlinear wave propagation of the uniform duct by using time-evolution in the wavenumber space.

3.1. Wavenumber space model

The acoustic behavior of propagating waves in the uniform duct can be understood as one-dimensional waves, of which the approximation is accurate up to the cut-off frequency of the first radial mode of the uniform circular duct [4]. The governing equations of one-dimensional acoustic waves are expressed with the conservation equations of the mass, momentum and energy, which support three characteristic waves: acoustic, entropy and vorticity. By decoupling the three

characteristics of the system, the governing equations can be simplified to a simple nonlinear equation for the acoustic wave. To investigate the phenomenon of nonlinear wave propagation in the uniform duct, this equation can be expressed as [32]

$$\frac{\partial p(x,t)}{\partial t}+\left(c_\infty+\frac{\gamma+1}{2}p(x,t)\right)\frac{\partial p(x,t)}{\partial x}=0, \tag{11}$$

where the dimensionless variables are set to be the same as those that are used in time–space domain analysis. By recasting Eq. (11) into a conservation form with these dimensionless variables, the following initial-value problem is obtained

$$\frac{\partial p(x,t)}{\partial t}+\frac{\partial p(x,t)}{\partial x}+\frac{\gamma+1}{4}\frac{\partial p^2(x,t)}{\partial x}=0, \tag{12}$$

with the initial condition,

$$p(x,0)=f(x). \tag{13}$$

According to the study of Tam and Shen [33], the nonlinear wave-steepening effect is not fully captured due to spurious spatial oscillations, when Eq. (12) is solved by using the finite difference method in time–space domains. By comparing this solution with the exact solution in the wavenumber space, Tam and Shen figured out that these oscillations are related to the size of the finite-difference stencil. Therefore, only the computation that uses a high-order finite-difference scheme or a large size of the finite-difference stencil can well describe the nonlinear wave propagation without numerical oscillations that generally entail a greater computational burden. To avoid this difficulty in time–space domain analysis for computing the nonlinear wave propagation in the uniform duct, the time-evolution of the exact solution of Eq. (12) in the wavenumber space is considered. The Fourier transformation of Eq. (12) leads to

$$\frac{\mathrm{d}P(\alpha,t)}{\mathrm{d}t}+\mathrm{i}\alpha\left[P(\alpha,t)+\frac{\gamma+1}{4}\int_{-\infty}^{\infty}P(k,t)P(\alpha-k,t)\,\mathrm{d}k\right]=0, \tag{14}$$

with the initial condition, $P(\alpha,0)=F(\alpha)$.

In Eq. (14), P and F denote the Fourier-transform pair of p and f, respectively, and α is wavenumber. Eq. (14) can be solved numerically by first discretizing the wavenumber axis into a fine mesh with spacing, $\Delta\alpha$, for converting the integral into sums. The discretization form of Eq. (14) is

$$\frac{\mathrm{d}P_n}{\mathrm{d}t}+in\,\Delta\alpha\left[P_n+\frac{\gamma+1}{4}\sum_{j=-N}^{N}P_jP_{n-j}\Delta\alpha\right]=0, \tag{15}$$

where $n=-N,\ -N+1,\ldots,N-1$ and N.

As in the time–space computation, Eq. (15), along with the initial condition, can be integrated by using Adams–Bashford's time-marching algorithm.

3.2. Computation of nonlinear wave propagation in the uniform duct

Problem 1. Nonlinear TLs of simple expansion mufflers for the incident nonlinear acoustic pulse.

To compute the TL of the uniform duct for nonlinear incident waves, the time-integration of Eq. (15) is conducted for the following initial condition:

$$P(\alpha,0)=\frac{1}{2\sqrt{\pi\ln 2}}hb\exp\left[-\frac{(\alpha b)^2}{4\ln 2}\right], \tag{16}$$

where h and b are the amplitude and bandwidth, respectively, of the Gaussian-shaped wave. The initial pulse matches the initial condition that is used in the time–space domain analysis. The initial condition, Eq. (16), in the discretized form is

$$P_n=\frac{1}{2\sqrt{\pi\ln 2}}hb\exp\left[-\frac{(n\Delta\alpha b)^2}{4\ln 2}\right]. \tag{17}$$

In Eq. (17), $h/\rho_\infty c_\infty^2=0.05$ and $b/\Delta x=10$, which are the same as for the computations in the time–space domain. The computed result is shown in Fig. 9 where it is clearly observed that the amplitudes of the wavenumber spectrum decrease for the components of wavenumbers below $80\,\mathrm{m}^{-1}$, whereas they increase for those above $80\,\mathrm{m}^{-1}$. Therefore, as time progresses from $t/(\Delta x/c_\infty)=0$ to 360, the energy-cascade process occurs from low wavenumbers to high wavenumbers.

To visualize the phenomenon of wave propagation in a spatial domain, the results from time-evolution in the wavenumber space are transformed into the spatial domain at every time-step, by using the inverse Fourier transform. The results are shown in Fig. 10. For obtaining a sufficient duration of recording until the wave totally exits the uniform duct, the length of the spatial domain is set up longer than the whole length of the expansion mufflers, i.e.,

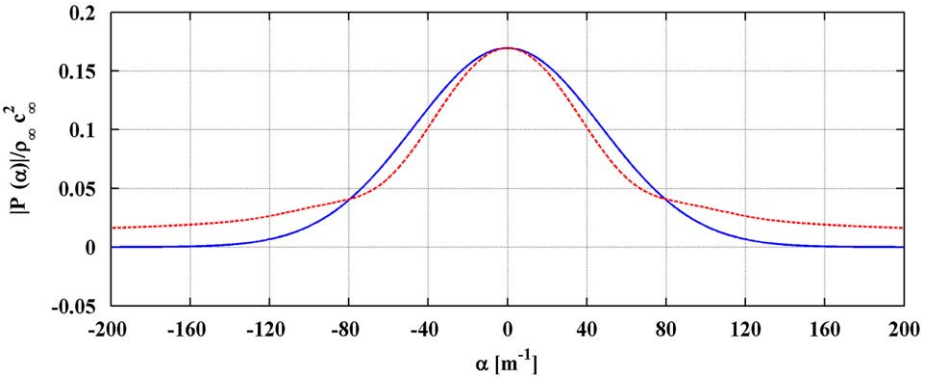

Fig. 9. Time-evolution of the wavenumber spectrum of an acoustic pulse ($h/\rho_\infty c_\infty^2=0.05$ and $b/\Delta x=10$) (——— $t/(\Delta x/c_\infty)=0$, — — — $t/(\Delta x/c_\infty)=360$).

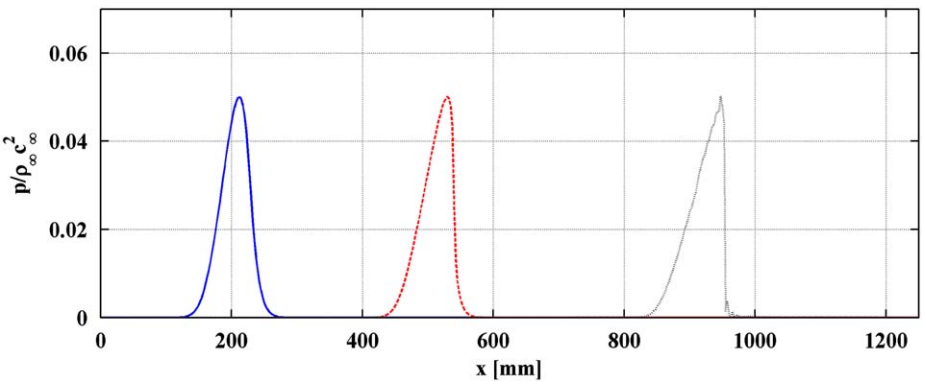

Fig. 10. Propagating waveform in the spatial domain at the incident time (———, $t/(\Delta x/c_\infty)=80$; — — —, $t/(\Delta x/c_\infty)=200$ and ……, $t/(\Delta x/c_\infty)=360$).

$0<x<1250$ mm. It can be seen in this figure that the nonlinear steepening process exactly matches that obtained by the time–space domain method, shown in Fig. 3. This nonlinear effect causes the TL of the uniform duct to be non-zero.

The time-history of pressure at the monitoring point at $x=800$ mm shown in Fig. 10 is utilized to compute the TL of the uniform duct. Fig. 11a presents the spectrums of the incident and transmitted waves. It can be seen from this figure how the energy cascade process is related to the nonlinear steepening process in the spatial domain shown in Fig. 10. Fig. 11b shows the corresponding TL, where it can be observed that the levels of TL in the frequency-range above 4400 Hz are lower than zero whereas, in the frequency-range below 4400 Hz, the levels of TL are greater than zero. These characteristics of the TL distribution can be fully understood in association with the energy cascade from lower-frequency components to higher-frequency ones.

By combining the nonlinear TL of the uniform duct with the linear TL of the muffler, the nonlinear TL of the muffler, using a hybrid model, is predicted in the form

$$\mathrm{TL}_{\mathrm{hybrid}}=\mathrm{TL}_{\mathrm{semi,muffler}}+\mathrm{TL}_{\mathrm{duct}}, \tag{18}$$

where TL_{duct} refers to the nonlinear TL of the uniform duct that is predicted by using time-evolution in the wavenumber space and $TL_{\mathrm{semi,muffler}}$ refers to the semi-analytic solution of the muffler. As described in Eq. (18), by simply adding the nonlinear TL of the uniform duct to the semi-analytic solution of the linear TL of a silencer, the nonlinear TL of such a silencer, which contains nonlinear effects due to the initial pulse that has acoustically high amplitude, can be effectively predicted.

Problem 2. Nonlinear acoustic wave propagation in a lined duct for high amplitude of sinusoidal wave.

To compute the nonlinear acoustic wave propagation in the duct without a liner for nonlinear sinusoidal waves, modeling the sinusoidal wave is first needed in the wavenumber space. The sinusoidal wave in time domain, $A\times\sin(kx-\omega t)$, can be represented in the wavenumber space through the Fourier transformation

$$P(\alpha,0)=\frac{iA}{2\pi}[\delta(\alpha+\alpha_0)-\delta(\alpha-\alpha_0)], \tag{19}$$

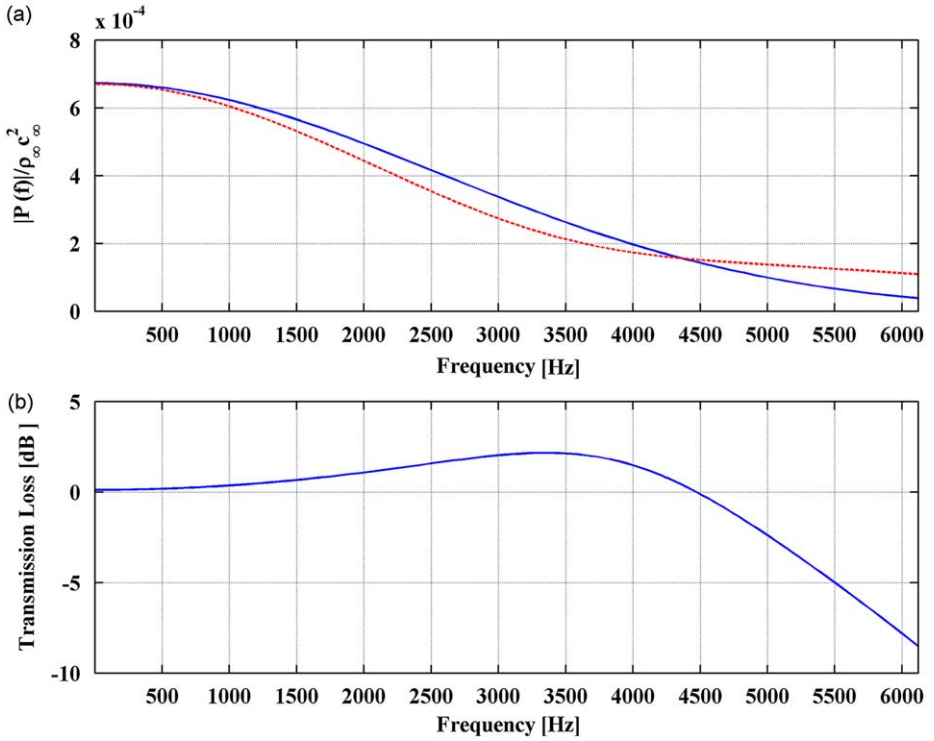

Fig. 11. (a) Spectrums of the incident/transmitted wave in the uniform duct (——— incident wave; — — — transmitted wave.) and (b) TL for the uniform duct.

where A denotes the amplitude of the wave of which the SPL is set to be 160 dB, equal to that in the nonlinear time-domain analysis. Here, α_0 represents the fundamental wavenumber for the 250 Hz, which is set to be $2\pi f/c_\infty$. Eq. (19) is modeled by Heaviside function (H) in the wavenumber space as follows:

$$P(\alpha,0)=\frac{iA}{2\pi}\lim_{\varepsilon\to 0}\frac{1}{\varepsilon}\{[H(\alpha_0-\varepsilon/2)-H(\alpha_0+\varepsilon/2)]-[H(-\alpha_0-\varepsilon/2)-H(-\alpha_0+\varepsilon/2)]\} \tag{20}$$

With initial condition of Eq. (20), Eq. (14) is computed through the time evolution in wavenumber domain. The results are shown in Fig. 12a. It can be seen that, as $t/(\Delta x/c_\infty)$ goes from 0 to 800, the harmonics for the fundamental are generated. The nonlinearity due to the high amplitude of source, shown in Fig. 4, can be also observed in Fig. 12a. With similar procedure applied for the Problem 1, the results from the time evolution in wavenumber space are transformed in the spatial domain using the inverse Fourier transformation. Subsequently, the time histories of the wave propagation are recorded at every point in spatial domain. The SPLs computed by using these time histories of data are shown in Fig. 12b.

By combining the nonlinear wave propagation with the linear wave propagation in a lined duct, the variation of SPL of the nonlinear wave in the lined duct is predicted by the following formula:

$$\mathrm{SPL}_{\mathrm{hybrid}}=\mathrm{SPL}_{\mathrm{Linear}}-\mathrm{SPL}_{\mathrm{ref}}+\mathrm{SPL}_{\mathrm{duct}}, \tag{21}$$

where $\mathrm{SPL}_{\mathrm{duct}}$ refers to the nonlinear wave propagation in the uniform duct that is predicted by using time-evolution in the wavenumber space, $\mathrm{SPL}_{\mathrm{Linear}}$ the linear solution of the lined duct, and $\mathrm{SPL}_{\mathrm{ref}}$ the reference SPL of the linear wave, which is $\mathrm{SPL}_{\mathrm{ref}}$=130 dB. As described in Eq. (21), by simply adding the nonlinear wave propagation in a uniform duct to the linear solution for a silencer, the nonlinear sound attenuation in a lined duct can be effectively predicted.

4. Comparison of predicted results

The nonlinear acoustic performances of the silencers are predicted by utilizing the hybrid method through the computations of nonlinear TLs of mufflers and nonlinear wave propagation in lined ducts. The results of nonlinear TLs of mufflers #1 and #2 are given in Fig. 13a and b, respectively.

The nonlinear sound attenuation performances that are computed through the hybrid method are compared with those that are yielded by the time–space method. It can be seen that both predictions are in good agreement. As described in Section 2.1, the dimensions of mufflers #1 and #2 differ so that the cut-off frequency of the first radial mode for muffler #1 is 6476 Hz, while that of muffler #2 is 2612 Hz. It can be seen in Fig. 13a that the comparison of TL is undertaken in the

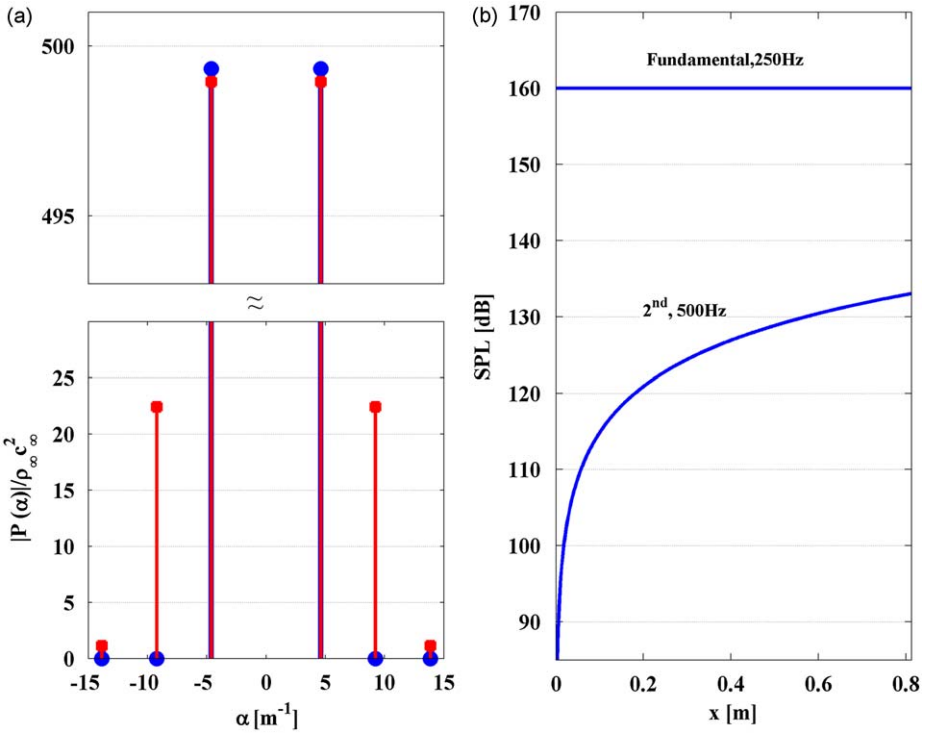

Fig. 12. Nonlinear wave propagation from wavenumber space model with fundamental frequency of 250 Hz for the amplitude of 160 dB: (a) time-evolution of the wavenumber spectrum (●: $t/(\Delta x/c_\infty)=0$, ■ $t/(\Delta x/c_\infty)=800$) and (b) SPL along the wall.

frequency-range that is below the first cut-off frequency, 6476 Hz, which means that only the plane wave is involved in the process of transmission loss. In Fig. 13b, where the comparison is undertaken in the frequency-range that is above the first cut-off frequency, 2612 Hz, the TL of muffler #2 may be affected by the higher modes in that frequency range. The hybrid method is based on the one-dimensional nonlinear wave propagation model. Consequently, the predicted TL for muffler #1 is expected to show closer agreement with that yielded by the time–space method than in the case of muffler #2. It can be gathered from Fig. 13a and b that the TL of muffler #1 that is predicted by the hybrid method conforms well to that yielded by the computations in the time–space domain. With regard to muffler #2, the higher modes seem to affect the level of the TL in the frequency-range that is above the first cut-off frequency, where the predicted TL from the hybrid method shows a slightly different shape when compared to that yielded by the time–space method. However, although the hybrid model is based on the one-dimensional propagation model, the predictions of the nonlinear TL from the hybrid model are satisfactory even in that frequency range where higher modes may affect the transmission process. Although radial modes of the chamber do not seem to contribute significantly to the nonlinear TL, their effect needs to be more clearly investigated; this remains a direction for future research.

The predicted nonlinear propagation in the lined duct for the harmonic incident waves at 250 and 1000 Hz are shown in Fig. 14a and b, respectively. The nonlinear absorption performances that are computed through the hybrid method are compared with those that are yielded by the time–space method. As shown in Fig. 14a, the predicted SPLs of the component at the fundamental frequency of 250 Hz are almost same for each other. This is because the nonlinear fundamental wave transfers negligible amount of its energy to harmonics during the propagation in the ducts as shown in Fig. 4 and 12b. Furthermore, it can be seen that the SPL variations of 2nd harmonic components predicted by the hybrid method well trace that by the time–space method. Although there are small differences in the SPL variations of 2nd harmonics between two results in the vicinity of $x=0.2032$ m, which corresponds to the entrance of the liner, the SPLs are very close to each other after that region. The reason for this small discrepancy of SPL variations of 2nd harmonic can be explained by using the amplitude variation of fundamental wave which gradually decreases until $x=0.4$ m. This indicates that the transferred energy to 2nd harmonic from the fundamental, computed by the time–space method, is less than that by the hybrid method. This absorption characteristics leads to the small difference in the initial variation of SPL between two results. However, the amplitude of the fundamental wave gradually increases to initial value of 160 dB. Consequently, the SPL variations predicted by two methods are in good agreement in the vicinity of the exit of liner. To more clearly illustrate the effect of the amplitude variation of the fundamental wave, the case of incident harmonic wave at the frequency of 1000 Hz with the amplitude of 160 dB is considered. The predicted results are shown in Fig. 14b. It can be seen that the amplitude of the fundamental wave component decreases by 55 dB after it passed the liner. Fundamental

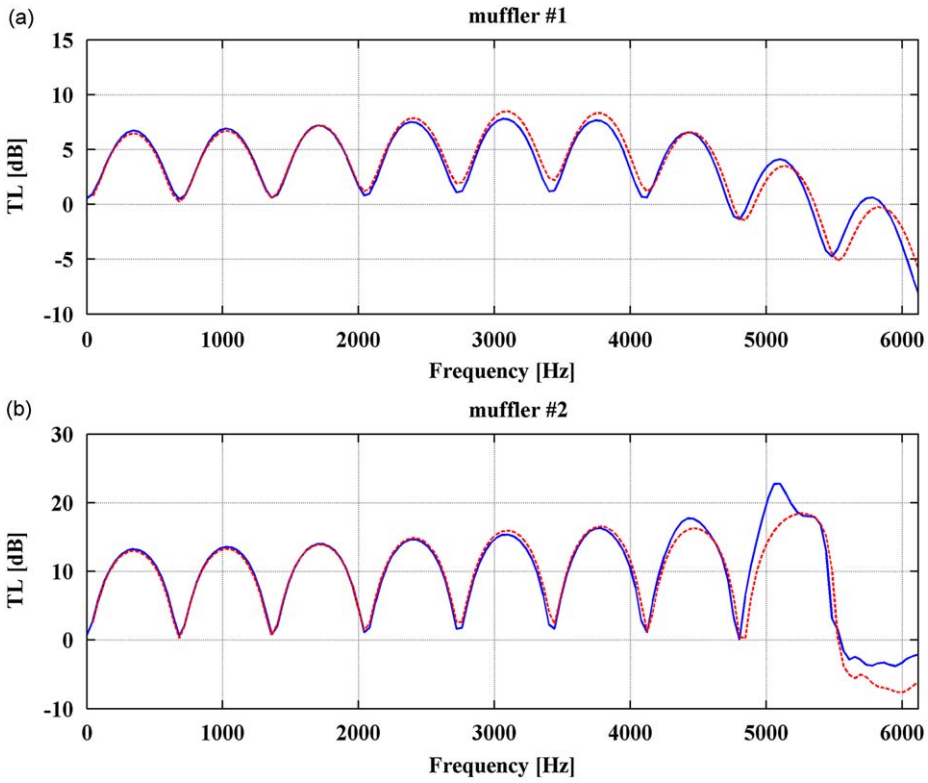

Fig. 13. Comparison of nonlinear TLs through time-domain analysis with those yielded by the hybrid method for (a) muffler #1 and (b) muffler #2 (c) (——— time-domain analysis; — — — hybrid method).

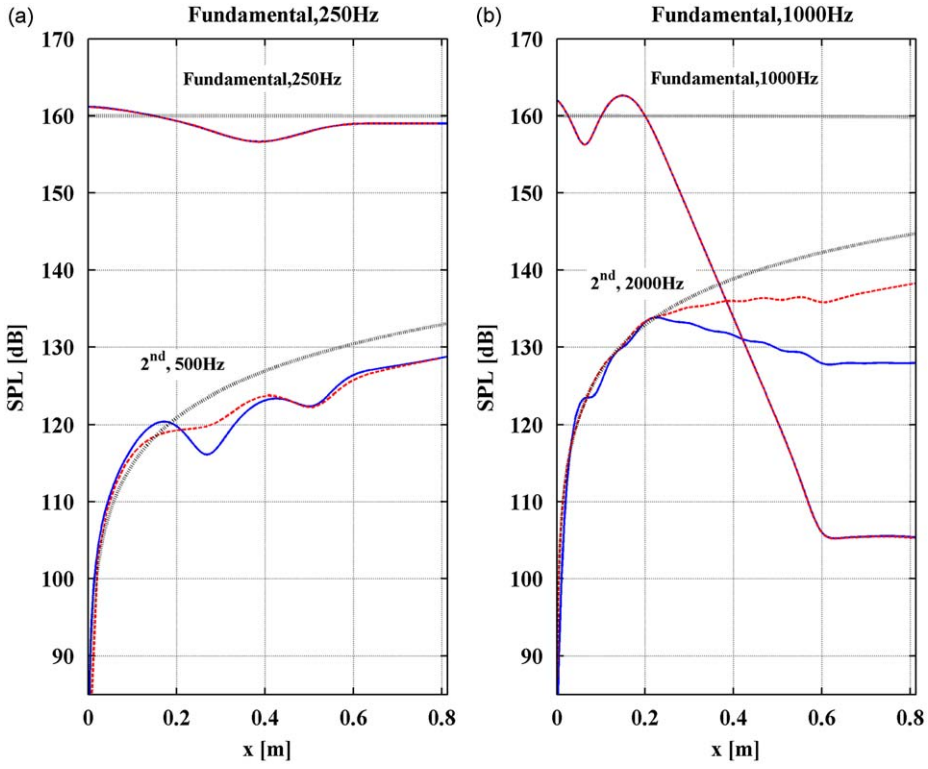

Fig. 14. Comparison of nonlinear wave propagations predicted by the time-space and hybrid methods: (a) fundamental wave with frequency of 250 Hz and (b) fundamental wave with frequency of 1000 Hz (——— time-domain analysis; — — — hybrid method; ■ ■ ■ without liner)).

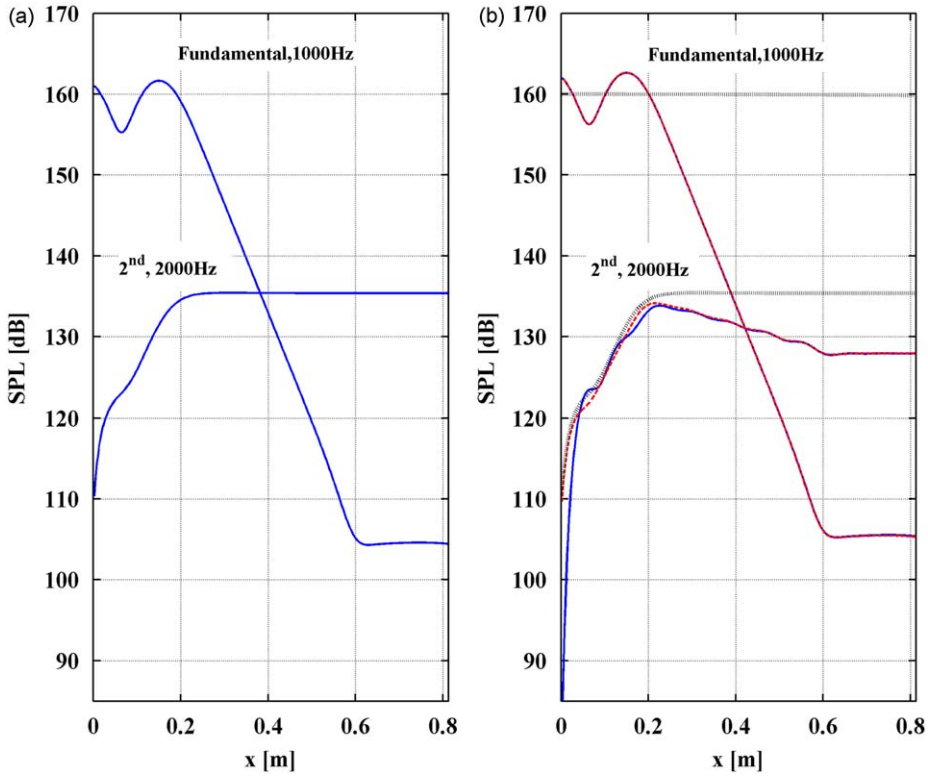

Fig. 15. Nonlinear wave propagation from the iterative hybrid method with fundamental frequency of 1000 Hz: (a) considering only the attenuation of the fundamental and (b) including the additional attenuation of 2nd harmonic (——— time-domain analysis; — — — iterative hybrid method; ■ ■ ■ without liner).

component mostly loses its acoustic energy during the propagation on the liner so that the difference in the SPL variation of 2nd harmonic predicted by the time–space and hybrid methods increases as the amplitude of fundamental wave decreases. The SPL predicted by the hybrid method is larger than that from the time–space method because the current algorithm of the hybrid method does not consider the change in the amplitude of the fundamental wave during the time-marching. One of the measures to correct this difference is to use the iterative hybrid method, where, at each time step during the time-marching of the nonlinear propagation in the wavenumber space, the decreased amplitudes of the fundamental wave are continuously updated by the amount corresponding to the linear loss by its interaction with the liner.

The SPLs of fundamental and 2nd harmonic predicted by using the iterative algorithm of the hybrid method are shown in Fig. 15a. In this case, the attenuation of 2nd harmonic by the liner is not considered. Since the attenuation of the SPL of the fundamental wave is only reflected to its amplitude in the wavenumber space, the pattern of decreased SPL of fundamental wave in Fig. 15a is exactly the same as the linear case shown in Fig. 7b. The variation of SPL of the 2nd harmonic predicted by the iterative hybrid method has different shape with that from the original hybrid method. As the amplitude of fundamental wave decreases to the value of linear level, its acoustic energy transferred to the 2nd harmonic is negligible. Subsequently, the amplitude of 2nd harmonic does not increase as shown in Fig. 15a. The generation and attenuation of 2nd harmonic are computed by utilizing iterative hybrid method as shown in Fig. 15b. It can be seen that the use of the modified hybrid method improves the agreements of its prediction with that by the time–space method.

Overall, these illustrative computations using the benchmark problems indicate that the hybrid model can be used as an alternative method of estimating the nonlinear acoustic performance of silencers, instead of the time–space computational aero-acoustic techniques that generally entail a greater computational burden.

5. Conclusion

The acoustic performances of silencers were investigated for both linear and nonlinear incident waves by using two model problems: one is the prediction of TL for a simple circular expansion mufflers and the other is the computation of the acoustic wave propagation in the lined duct.

Through the computations in the time–space domain that use high-order finite-difference methods, the mechanism of the nonlinear sound attenuation of the silencers is found to be possibly decoupled into two distinct processes: a linear sound attenuation that is due to a mismatch in the impedance and sound absorbing material; a phenomenon of energy-cascade through nonlinear wave propagation.

Based on this observation, a hybrid model, which is composed of two individual computations, is proposed for effectively predicting the nonlinear sound attenuation of a silencer. The method computes the sound attenuation of the silencer in a linear regime and predicts the nonlinearity of one-dimensional nonlinear wave propagation. The latter is carried out by utilizing the integration of nonlinear time evolution in the wavenumber domain. The final prediction is established by combining these two individual results. The validity of the hybrid model is shown by comparing its predictions with those yielded by high-order, finite-difference methods in the time–space domain. For the first model problem, it is revealed that the predicted TL of simple expansion mufflers for the nonlinear incident wave from the hybrid methods shows a good agreement with those from the time–space computation. Moreover, it is shown that the present model may be applied for predicting the TL of silencers in a frequency-range where radial modes are involved. For the second model problem, the predicted SPL variation along the duct wall from the present method closely follows that by time–space methods. However, if the reduction of the amplitude of fundamental incident harmonic wave is significant such that the transferred energy from fundamental to higher harmonics is negligible, there is noticeable difference between two computations. In this case, however, it is shown that the agreement of the predictions is improved by using the iterative algorithm of the hybrid method. Overall, these results confirms that the hybrid model is an effective alternative for predicting nonlinear acoustic performance of a silencer in lieu of the time–space domain computation for which the computational burden is generally high.

Acknowledgement

This work was supported by the National Research Foundation of Korea (NRF) grant funded by the Korea government (MEST) (No. 2009-0052961).

Appendix A

With the use of the liner (CT57) used in NASA Langley flow impedance tube, the acoustical material is modeled. The impedance boundary condition is usually used in frequency domain and cannot be directly implemented in time-domain. For the broadband time-domain impedance boundary condition, we followed the procedure suggested by Özyörük et al. [29].

The impedance boundary condition in frequency domain is written in the form

$$\mathrm{i}\omega\widehat{p}(\omega,\mathbf{x})+\mathbf{V}_0(\mathbf{x})\cdot\nabla\hat{p}(\omega,\mathbf{x})-\mathbf{n}\cdot[\mathbf{n}\cdot\nabla\cdot\mathbf{V}_0(\mathbf{x})]\hat{p}(\omega,\mathbf{x})=-[\mathrm{i}\omega Z(\omega)][\mathbf{n}\cdot\widehat{v}(\omega,\mathbf{x})] \tag{A.1}$$

where $\widehat{p}$ and $\widehat{v}$ are the complex amplitude of the pressure and velocity perturbations, respectively, $\mathbf{n}$ is the normal vector to the surface, $\mathbf{V_0}$ denotes the mean velocity and ω is angular frequency. $Z(\omega)$ is the impedance of the acoustic absorbing material which is given by $Z(\omega)=R(\omega)+\mathrm{i}X(\omega)$, where $R(\omega)$ and $X(\omega)$ denote the resistance and reactance of the impedance. With absence of the mean velocity, $\mathbf{V_0}=0$, Eq. (A.1) can be simplified into

$$\widehat{p}(\omega,\mathbf{x})=-Z(\omega)\widehat{v}(\omega,\mathbf{x}) \tag{A.2}$$

To predict the attenuation of broadband acoustic wave by a acoustic liner, we use the fitted impedance function $Z(\omega)$ in the form

$$\frac{Z(\omega)}{\rho_\infty c_\infty}=r_1+\mathrm{i}\omega r_7+\frac{r_2-r_1}{1+\mathrm{i}\omega r_3}+\frac{\mathrm{i}\omega r_4}{(1-(\mathrm{i}\omega r_6)^2)+r_5}, \tag{A.3}$$

where r_i (i=1,2,…,7) is given in the left column of Table 1. The fitted impedance function $Z(\omega)$ is compared with experimental data in Fig. A1. Note that the NASA experiment was conducted for the source level of 130 dB.

Özyörük et al. [29] implemented the time-domain impedance boundary condition by utilizing z-transformation. Using the time-shifting theorem and first order backward difference approximation, the time derivative operator can be written as

$$\mathrm{i}\omega\equiv\frac{\partial}{\partial t}\equiv\frac{1-z^{-1}}{\Delta t} \tag{A.4}$$

Substituting Eq. (A.4) into Eq. (A.3), the impedance boundary condition in z-domain can be written as [29]

$$Z(z)=\frac{a_0+\sum_{l=1}^{4}a_l z^{-l}}{1-\sum_{k=1}^{3}b_k z^{-k}} \tag{A.5}$$

The coefficients in Eq (A.5), a_l and b_k, depend on the computation time interval as given in Eq. (A.4). In present study, time interval, Δt is set to be $0.1/(\Delta x/c_\infty)$. The calculated coefficients are represented in the right column of Table A1.

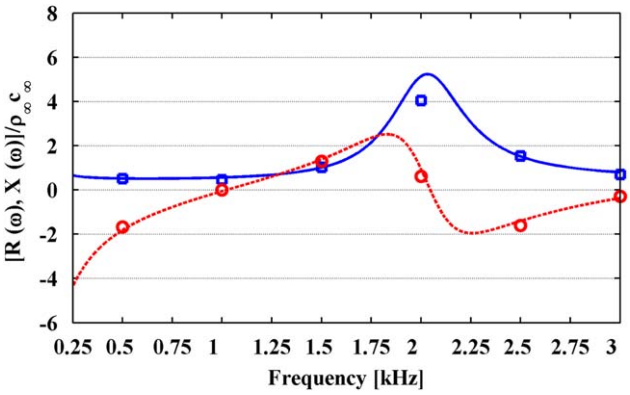

Fig. A1. The acoustic impedance of the NASA CT57 liner (——— $R(\omega)_{\text{fitted}}$; — — — $X(\omega)_{\text{fitted}}$; □ $R(\omega)_{\text{exp}}$; ○ $X(\omega)_{\text{exp}}$).

Table A1
Coefficients of impedance function in frequency domain and z-domain of CT57 liner.

Frequency domain [15]	z-domain
$r_1=4.539433460495040\times10^{-1}$	$a_0=222.327216160491$
$r_2=1.099477558604532\times10^{2}$	$a_1=-888.642771798514$
$r_3=1.518314688928225\times10^{-2}$	$a_2=1331.97488133121$
$r_4=8.336386582323006\times10^{-5}$	$a_3=-887.330303197786$
$r_5=1.745180668436959\times10^{-5}$	$a_4=221.670977536078$
$r_6=7.831410850410846\times10^{-5}$	$b_1=2.99910165399067$
$r_7=6.629909782342582\times10^{-5}$	$b_2=-2.99821787229708$
	$b_3=0.999116218020116$

The relation between the velocity and pressure perturbations in Eq. (A.2) is also transformed in z-domain

$$P(z)=-Z(z)V(z) \tag{A.6}$$

With Eqs. (A.5) and (A.6) can be written by

$$P(z)(1-b_1z^{-1}-b_2z^{-2}-b_3z^{-3})=-V(z)(a_0+a_1z^{-1}+a_2z^{-2}+a_3z^{-3}+a_4z^{-4}) \tag{A.7}$$

Through the inverse z-transformation, Eq. (A.7) is written as

$$p^n-b_1p^{n-1}-b_2p^{n-2}-b_3p^{n-3}=-(a_0v^n+a_1v^{n-1}+a_2v^{n-2}+a_3v^{n-3}+a_4v^{n-4}), \tag{A.8}$$

where the superscript, n, represents the nth time. In Eq. (A.8), p^n has a implicit relation with v^n. To explicitly implement Eq. (A.8) in time-domain and thus determine p^n, the linear momentum equation in the y-direction is utilized. The velocity, v^n, is also determined using the momentum equation with nth time pressure, p^n. Insertion of the momentum equation in Eq. (A.8) leads to the final form of the time-domain impedance boundary condition

$$p^n-b_1p^{n-1}-b_2p^{n-2}-b_3p^{n-3}=-\left(a_0\left(-\frac{\partial p^n}{\partial y}\Delta t+v^{n-1}\right)+a_1v^{n-1}+a_2v^{n-2}+a_3v^{n-3}+a_4v^{n-4}\right) \tag{A.9}$$

and its discretized form

$$p^n_{i,JW}=\left[\sum_{k=1}^{3}b_kp^{n-k}_{i,JW}-\left(a_0\left(-\frac{\Delta t}{\Delta y}\sum_{j=1}^{6}a_j^{06}p^n_{i,JW+j}+v^{n-1}_{i,JW}\right)+\sum_{l=1}^{4}a_lv^{n-l}_{i,JW}\right)\right]\Big/\left(1-\frac{a_0^{06}a_0\,\Delta t}{\Delta y}\right) \tag{A.10}$$

where i and JW denote the x-direction grid number and the location of impedance boundary, respectively. The coefficient, a_j^{06}, represents the DRP coefficient of backward stencil [18].

The time-domain impedance model is validated by the comparison with NASA experimental data as shown in Fig. 7.

Appendix B

For the Euler equations, the slip condition that the normal velocity, u, is zero is required on the wall as the physical boundary condition. However, the use of high-order finite difference equations, instead of partial differential equations, requires additional numerical boundary conditions on the wall to suppress the spurious waves. In this work, the technique of using ghost values of the pressure at ghost points [19] is utilized with regard to the numerical boundary conditions.

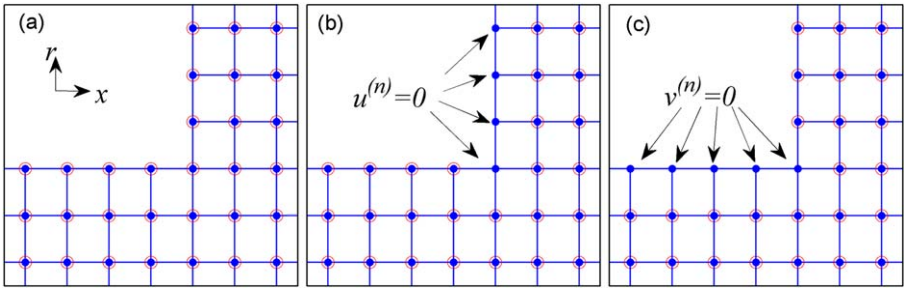

Fig. B1. Grid points in a discontinuous region for which the selective damping term is applied for the variables: (a) p and ρ; (b) u and (c) v (● grid point; O grid points where the selective damping term is effective).

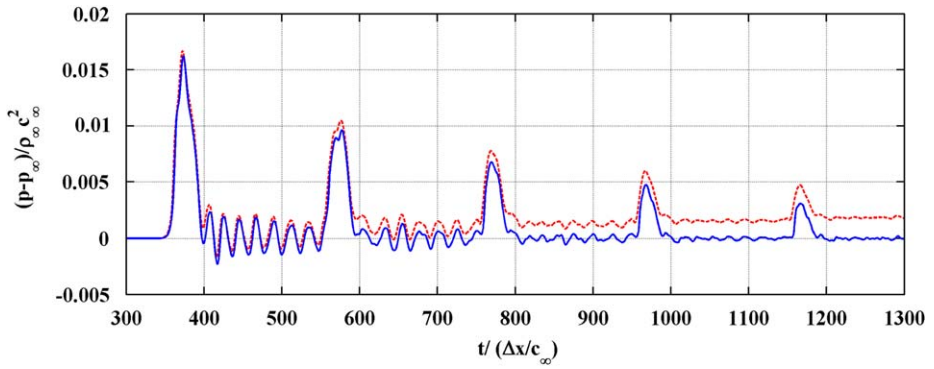

Fig. B2. Comparison of the pressure fluctuation at x=400 mm for muffler #1 between two cases: (case 1) application of damping terms at every grid point for all variables; (case 2) application of damping terms with a different strategy, as shown in Fig. B1 (— — — case 1, ——— case 2).

Through the preliminary numerical tests, we find that the wrong application of these numerical wall-boundary conditions in association with the artificial numerical damping generates a low-frequency noise that is embedded in the transmitted waves at the outflow boundary, as shown in Fig. B2 (dashed line). Intensive test simulations show that this low-frequency noise is due to the non-zero normal velocity on the wall, which is caused by the miscalculated ghost-values of the pressure. This occurs because the damping term is included to compute the ghost values of pressure. Therefore, the damping term in the momentum equation in the direction that is normal to the wall is not applied for the grid points on the wall, as shown in Fig. B1. Fig. B2 shows the comparison between two cases of the time-history of pressure fluctuations that is predicted at x=400 mm, as shown in Fig. 1, for muffler #1: in the first case, the damping term is applied on all grid points for all variables and in the second case, a different strategy, as shown in Fig. B1, is applied for the numerical damping terms. It is clearly seen in Fig. B2 that the mean level of the pressure fluctuation in the former case gradually increases with time, while in the latter case, it retains the same value as the initial mean pressure.

References

[1] M.L. Munjal, *Acoustics of Ducts and Mufflers*, 1st ed., Wiley, New York, 1987.
[2] M.L. Munjal, A simple numerical method for three-dimensional analysis of simple expansion chamber mufflers of rectangular as well as circular cross-section with a stationary medium, *Journal of Sound and Vibration* 116 (1987) 71–88.
[3] M. Abom, Derivation of four-pole parameters including higher order mode effects for expansion chamber mufflers with extended inlet and outlet, *Journal of Sound and Vibration* 137 (1990) 403–418.
[4] L.J. Eriksson, Higher order mode effects in circular ducts and expansion chambers, *Journal of the Society of America* 68 (2) (1980) 545–550.
[5] D.F. Ross, A finite element analysis of perforated component acoustic system, *Journal of Sound and Vibration* 79 (1) (1981) 113–143.
[6] T. Morel, J. Morel, D.A. Blaser, Fluid dynamic and acoustic modeling of concentric tube resonators/silencers, SAE, No. 910072, 1991.
[7] S.M. Sapsford, V.C.M. Richards, D.R. Amelee, T. Morel, M.T. Chapell, Exhaust system evaluation and design by non-linear modeling, SAE, No. 920686, 1992.
[8] A. Onorati, Prediction of the acoustical performances of muffling pipe systems by the methods of characteristics, *Journal of Sound and Vibration* 171 (3) (1994) 369–395.
[9] A. Onorati, G. Ferrari, Calculation of complex silencer performances by non-linear fluid dynamic simulation models, *Proceedings of the International Conference Inter-Noise* '94, Yokohama, Japan, 1994, pp. 1631–1634.
[10] A. Selamet, N.S. Dickey, J.M. Novak, A time domain computational simulation of acoustic silencers, *Journal of Vibration and Acoustics* 117 (1995) 323–331.
[11] C. Hwang, D.J. Lee, K.S. Chae, Time accurate finite difference method for performance prediction of a silencer with mean flow and nonlinear incident wave, *Journal of Mechanical Science and Technology* 21 (1) (2007) 1–11.
[12] C.K.W. Tam, H. Ju, M.G. Jones, W.R. Watson, T.L. Parrott, A computational and experimental study of slit resonators, *Journal of Sound and Vibration* 284 (2005) 947–984.

[13] R.C.K. Leung, R.M.C. So, M.H. Wang, X.M. Li, In-duct orifice and its effect on sound absorption, *Journal of Sound and Vibration* 299 (2007) 990–1004.
[14] N.S. Dickey, A. Selamet, J.M. Novak, The effect of high-amplitude sound on the attenuation of perforated tube silencers, *Journal of the Acoustical Society of America* 180 (3) (2000) 1068–1081.
[15] C.H. Cho, D.J. Lee, Time domain simulation of nonlinear acoustic propagation in a lined duct, *29th AIAA Aeroacoustics Conference*, 2008, pp. 2008–2830.
[16] C.K.W. Tam, Computational aeroacoustics: issues and methods, *AIAA Journal* 33 (1995) 1788–1796.
[17] Sanjiva K. Lele, Computational aeroacoustics: a review, AIAA Paper, 97-0018, 1997.
[18] C.K.W. Tam, JayC. Webb, Dispersion-relation-preserving finite difference schemes for computational acoustics, *Journal of Computational Physics* 107 (1993) 262–281.
[19] C.K.W. Tam, Z. Dong, Wall boundary conditions for high order finite difference schemes in computational aeroacoustics, *Theoretical and Computational Fluid Dynamics* 8 (6) (1994) 303–322.
[20] C. Cheong, S. Lee, The effects of discontinuous boundary conditions on the directivity of sound from a piston, *Journal of Sound and Vibration* 239 (3) (2001) 423–443.
[21] C. Cheong, P.F. Joseph, Y. Park, S. Lee, Computation of aeolian tone from a circular cylinder using source models, *Applied Acoustics* 69 (2) (2008) 110–126.
[22] C. Cheong, J. Ryu, S. Lee, Computation of aeolian tones from twin-cylinders using immersed surface dipole sources, *Journal of Mechanical Science and Technology* 20 (12) (2006) 2292–2314.
[23] C.W. Lim, C. Cheong, S. Shin, S. Lee, Time-domain computation of noise reduction by diffraction and finite impedance of barriers, *Journal of Sound and Vibration* 268 (2) (2003) 385–401.
[24] C. Cheong, S. Lee, Grid-optimized dispersion-relation-preserving schemes on general geometries for computational aeroacoustics, *Journal of Computational Physics* 174 (2001) 248–276.
[25] F.Q. Hu, A stable, perfectly matched layer for linearized Euler equations in unsplit physical variables, *Journal of Computational Physics* 173 (2001) 455–480.
[26] F.Q. Hu, X.D. Li, D.K. Lin, A stable, absorbing boundary conditions for nonlinear Euler equation and Navier–Stokes equations based on the perfectly matched layer technique, *Journal of Computational Physics* 227 (2008) 4398–4424.
[27] C.K.W. Tam, Laurent Lin, Time-domain impedance boundary condition for computational aeroacoustics, *AIAA Journal* 34 (5) (1996) 917–923.
[28] K.Y. Fung, H. Ju, Impedance and its time domain extensions, *AIAA Journal* 38 (1) (2000) 30–38.
[29] Y. Özyörük, L.K. Long, M.G. Jones, Time-domain numerical simulation of a flow-impedance tube, *Journal of Computational Physics* 146 (1998) 29–57.
[30] J.H. Bin, M.Y. Hussaini, Broadband impedance boundary conditions for the simulation of sound propagation in the time domain, *Journal of Acoustical Society of America* 125 (2) (2009) 664–675.
[31] M.G. Jones, W.R. Watson, T.L. Parrott, Benchmark data for evaluation of aeroacoustic propagation codes with grazing flow, *AIAA Paper*, 2005, pp. 2005–2853.
[32] C.K.W. Tam, Numerical methods in computational aeroacoustics, *AIAA short course*, 1997.
[33] C.K.W. Tam, H. Shen, Direct computation of nonlinear acoustic pulses using high-order finite difference schemes, AIAA Paper, 93-4325, 1993.